JGR Atmospheres

RESEARCH ARTICLE
10.1029/2022JD036880

High Flux of Small Sulfate Aerosols During the 1970s Reconstructed From the SE-Dome Ice Core in Greenland

Y. Iizuka[1], R. Uemura[2], H. Matsui[2], N. Oshima[3], K. Kawakami[1,4], S. Hattori[5,6], H. Ohno[7], and S. Matoba[1]

[1]Institute of Low Temperature Science, Hokkaido University, Sapporo, Japan, [2]Graduate School of Environmental Studies, Nagoya University, Nagoya, Japan, [3]Meteorological Research Institute, Tsukuba, Japan, [4]Graduate School of Environmental Science, Hokkaido University, Sapporo, Japan, [5]International Center for Isotope Effects Research, School of Earth Sciences and Engineering, Nanjing University, Nanjing, China, [6]Department of Chemical Science and Engineering, School of Materials and Chemical Technology, Tokyo Institute of Technology, Kanagawa, Japan, [7]Kitami Institute of Technology, Kitami, Japan

Key Points:

- Ice core analyses provide the first evidence of past seasonal deposition flux of large sulfate salt particles and small sulfates
- Compared to the 1970s, the small sulfates (<0.4 μm) aerosol flux significantly decreased in the 2010s
- Small sulfates were efficiently activated as cloud condensation nuclei during anthropogenic sulfate maximum (1970s)

Supporting Information:

Supporting Information may be found in the online version of this article.

Correspondence to:

Y. Iizuka,
iizuka@lowtem.hokudai.ac.jp

Citation:

Iizuka, Y., Uemura, R., Matsui, H., Oshima, N., Kawakami, K., Hattori, S., et al. (2022). High flux of small sulfate aerosols during the 1970s reconstructed from the SE-Dome ice core in Greenland. *Journal of Geophysical Research: Atmospheres*, *127*, e2022JD036880. https://doi.org/10.1029/2022JD036880

Received 2 APR 2022
Accepted 24 JUL 2022

Author Contributions:

Conceptualization: Y. Iizuka
Data curation: Y. Iizuka, R. Uemura, H. Matsui, N. Oshima, K. Kawakami, S. Hattori, H. Ohno
Formal analysis: Y. Iizuka, R. Uemura, H. Matsui, N. Oshima
Funding acquisition: Y. Iizuka, S. Matoba
Investigation: Y. Iizuka
Methodology: Y. Iizuka, H. Matsui, N. Oshima, K. Kawakami
Project Administration: Y. Iizuka
Validation: Y. Iizuka, R. Uemura

Abstract Aerosols significantly affect Earth's radiation budget, thus influencing global climate. In the Arctic, sulfate aerosols are thought to have reduced the warming during the twentieth century. However, trends in past sulfate aerosols are poorly known, especially the aerosol sizes and compositions. Here, we analyze a high-resolution ice core from southeastern Greenland, comparing the seasonal deposition flux of large sulfate salt particles and small sulfur compounds, including non-neutralized sulfuric acid, between the anthropogenic sulfate maximum (1973–1975) and after sulfur emissions control (2010–2012). Between these periods, we find that the large-diameter (>0.4 μm) flux remains roughly unchanged, yet the small-diameter (<0.4 μm) aerosol flux significantly decreases. The results indicate that small sulfates were efficiently activated as cloud condensation nuclei during the 1970s, and thus likely increased cloud albedo, offsetting the warming.

Plain Language Summary Sulfate aerosol compositions and size distributions are important factors in Earth's radiation budget. However, we have little information on past sulfate aerosol sizes and compositions over the Arctic due to a lack of reliable observations, and as such, we have less confidence in modeling historical aerosol composition and transport. We present here the first observational evidence that small sulfate particles increased in the Arctic during the 1970s. With emission controls, anthropogenic SO_2 emissions from eastern North America and Western Europe decreased after the 1980s, thus increasing the relative importance of large sulfate particles. Thus, our findings should help to improve the understanding of aerosol-cloud interactions, and provide new constraints for the parameterization in the model.

1. Introduction

Aerosols have had a large role in both global and regional climate change during the twentieth century (Shindell & Faluvegi, 2009). Sulfate aerosols can act as cloud condensation nuclei (CCN), increasing cloud albedo and thus cooling Earth's surface (Szopa et al., 2021). Due to increasing anthropogenic SO_2 emissions, sulfate aerosol in the Arctic increased until 1975 (Chylek et al., 2016; Szopa et al., 2021). Then, starting in the 1970s, the emissions decreased due to clean-air regulations in the Northern Hemisphere. As a result, a large aerosol contribution to mid-twentieth century Arctic cooling may account for the lack of an observed polar warming amplification at least until the 1970s (Polyakov et al., 2002). The rapid warming after the 1970s is likely to be partly due to the unintended consequences of clean-air policies that have greatly decreased sulfate precursor emissions from North America and Europe (Aizawa et al., 2022; Gillett et al., 2021; Shindell & Faluvegi, 2009; Takemura, 2020). However, even in recent model simulations, aerosols and clouds remain a major uncertainty in estimates of effective radiative forcing and climate projections (Oshima et al., 2020; Smith et al., 2020). Thus, more direct evidence of the role of sulfate aerosols on Arctic climate is needed. For example, even if the sulfate aerosol flux is fixed, the size of the sulfate aerosol will change the number density, and through the CCN effect, have a significant impact on cloud albedo.

Aerosols in the Arctic region contain anthropogenic and natural sulfates, mostly ammonium sulfate ($(NH_4)_2SO_4$) and sulfuric acid (H_2SO_4) from marine biological activity and anthropogenic SO_x emissions (Fisher et al., 2011; Seguin et al., 2011; Udisti et al., 2016). In the Arctic, the anthropogenic SO_2 dissolves in water droplets, forming sulfuric acid aerosol (hereafter, referred to as SO_4^{2-}). The $(NH_4)_2SO_4$ arises mostly from the reaction of H_2SO_4

Visualization: Y. Iizuka, R. Uemura, H. Matsui, N. Oshima, K. Kawakami
Writing – original draft: Y. Iizuka, R. Uemura, H. Matsui, N. Oshima, S. Hattori, S. Matoba

with ammonia (NH_3), which comes mainly from terrestrial biological activity and agricultural activities. The $(NH_4)_2SO_4$ salts form via condensational growth from SO_2 and NH_3 gases as well as by aqueous-phase reactions of SO_2 and NH_3 in water drops. As a result, the $(NH_4)_2SO_4$ aerosols generally exist in the nucleation and small accumulation modes smaller than 0.45 μm (Seguin et al., 2011). Aerosols in the Arctic region also contain sodium sulfate (Na_2SO_4) and calcium sulfate ($CaSO_4$). The Na_2SO_4 derives mostly from the reaction of NaCl from sea salt with H_2SO_4 (Park et al., 2004), or possibly from mirabilite formed on sea ice (Seguin et al., 2014). The $CaSO_4$ derives from terrestrial gypsum and also from a reaction in aerosol between H_2SO_4 and calcium carbonate ($CaCO_3$) (Li et al., 2006). A potential source region of $CaSO_4$ and $CaCO_3$ is the Asian highlands such as the Taklamakan and Gobi deserts (Bory et al., 2002, 2014). Such $CaSO_4$ can form from the reaction of $CaCO_3$ with H_2SO_4 from China (Seguin et al., 2011). The Na_2SO_4 and $CaSO_4$ aerosols generally occur in the coarse mode because they form on coarse sea salt (Seguin et al., 2011) and dust. In the Arctic, wet deposition produces about 90% of the black carbon, sulfate, and dust depositions (Breider et al., 2014). Thus, recent aerosols in the Arctic region are well-known to contain anthropogenic and natural sulfates; however, the characteristics of sulfur compounds during the mid-twentieth century have seen little study (Boucher & Anderson, 1995; Brock et al., 1990). The anthropogenic sulfate mass mainly resides in the accumulation mode (0.1–1.0 μm), with the sulfate aerosol only interacting with gas-phase ammonia and water vapor (Boucher & Anderson, 1995). Research is needed to determine the fraction of anthropogenic sulfate that forms on large-mode particles (over 1.0 μm) (Boucher & Anderson, 1995). Thus, the past variations of size distribution and CCN activity should be reconstructed to better elucidate aerosol's radiative effects.

Aerosols and their precursor emissions for climate models are available from databases such as AeroCom (Schulz et al., 2006, 2009), EDGAR (Crippa et al., 2016), and the Community Emissions Data System (Hoesly et al., 2018), all of which cover from the industrial revolution to the present. On the other hand, information on the chemical forms and size distribution of past aerosols is limited. In the atmosphere, H_2SO_4 formed from oxidation of SO_2 can exist either as gas, liquid, or salt (e.g., $(NH_4)_2SO_4$, Na_2SO_4, and $CaSO_4$) after reaction-neutralization with cations, which changes the aerosols' CCN activity properties. Aerosol composition and size distribution remain a large uncertainty for accurately predicting CCN number concentrations and determining cloud-base supersaturation (Moore et al., 2011).

Although aerosol deposition fluxes have been obtained from ice cores (Fischer et al., 2007; Wolff et al., 2006), most such studies retrieve the total sulfate ion flux, which combines both sulfate salts and sulfuric acid (Fischer et al., 1998). However, the total sulfate amount alone cannot reveal the number concentrations, size distribution, and CCN activity. One tool that can provide details of aerosol size and CCN activity is the sublimation-SEM/EDS method. This method has reconstructed aerosol size and compositions in surface snow (Iizuka, Ohno, et al., 2016; Iizuka, Tsuchimoto, et al., 2012) and ice cores (Iizuka et al., 2009; Iizuka, Uemura, et al., 2012), showing that the sulfate-salt flux is high during glacial periods and low during interglacial periods in inland Antarctica (Iizuka, Uemura, et al., 2012). However, there has not yet been an examination of how the sulfate chemical composition of single particles responded to the reduction in air pollution after the 1980s. In this study, we applied the sublimation-SEM/EDS method to an ice core from SE-Dome, a dome in southeast Greenland (67.18°N, 36.37°W, 3,170 m a.s.l.) (Iizuka, Matoba, et al., 2016). This dome area has an extremely high accumulation rate, meaning that its ice-core record has both a high time resolution (Iizuka et al., 2017) and negligible post-depositional chemical changes (Iizuka et al., 2018). In addition, a precise age scale (uncertainty of ±2 months) has already been established by matching oxygen isotope ($\delta^{18}O$) data from SE-Dome with those from isotope-enabled climate models (Furukawa et al., 2017). Thus, the SE-Dome ice core is one of the best ice cores to accurately determine the flux of past deposited aerosols.

The focus here is on the sulfur compounds in single particles, with comparison of the periods 1973–1975, the "1970s," and 2010–2012, the "2010s." The former period is the anthropogenic sulfate maximum, the latter period represents the period after widespread regulation of sulfur emissions. By comparison of the mass ratio of sulfate salt and insoluble dust from the sublimation method, and the ratio of sulfate ions and dust from liquid analyses (see Methods), we can divide the sulfate ion concentration into large particles of sulfate salt larger than 0.4 μm diameter and small sulfur compounds below 0.4 μm (Figure 1). This cutoff is a convenient filter pore size that we have used in previous studies (Iizuka, Uemura, et al., 2012). After analyzing their seasonal fluxes, we discuss their contributions to aerosol-cloud interactions and how they may improve aerosol climate models.

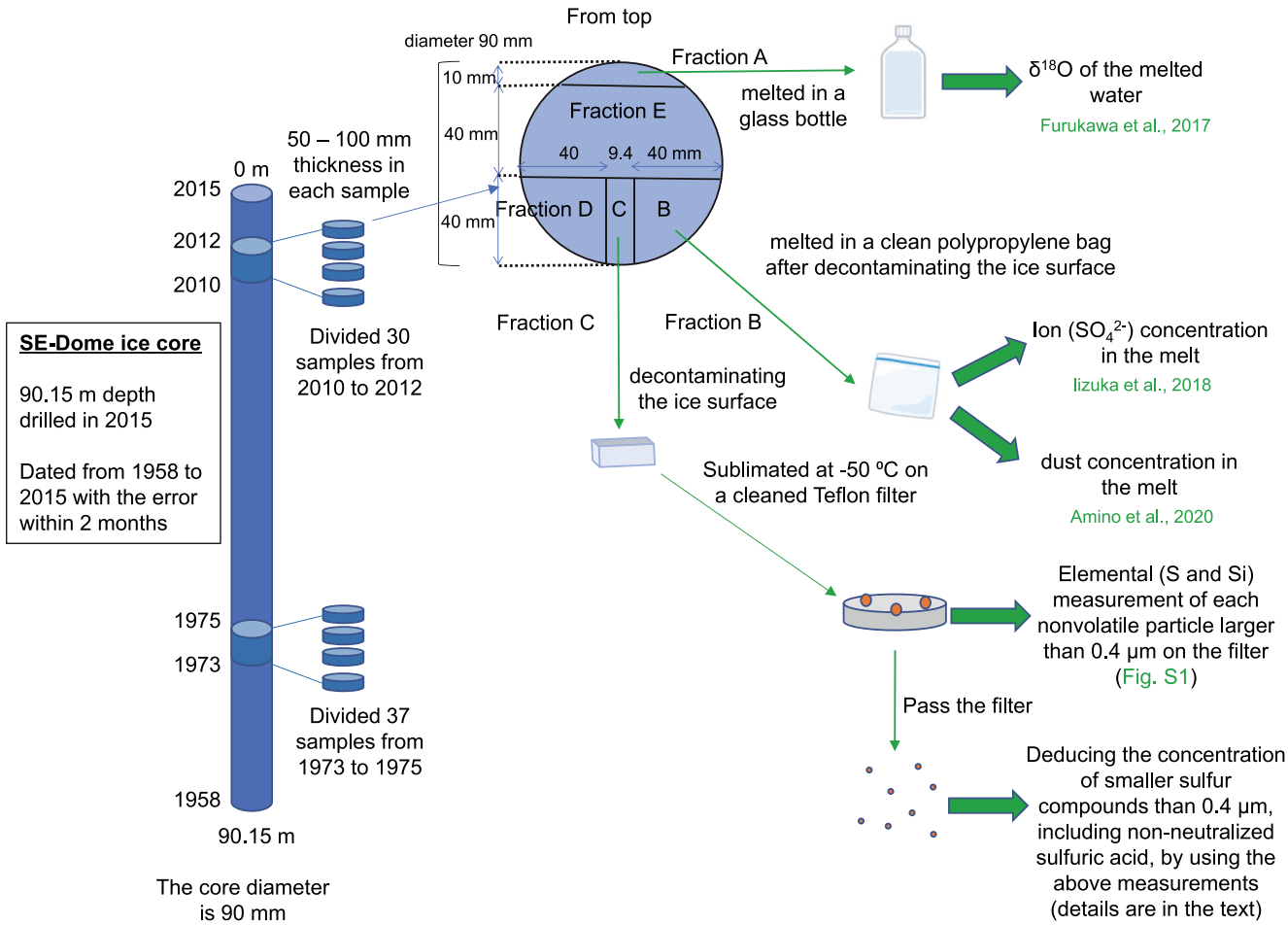

Figure 1. Overall analytical procedure. Fractions D and E are not used in this study.

2. Materials and Methods

2.1. Sampling Site and the SE-Dome Ice Core

The ice core samples came from SE-Dome in southeast Greenland (Iizuka, Matoba, et al., 2016). The timescale for this ice core was previously obtained by matching isotope models and has an uncertainty of less than 2 months (Furukawa et al., 2017). Thus, we can estimate the age of each ice section to seasonal resolution. In addition, as the accumulation rate is about 1 m yr^{-1} in water equivalent, impurity concentrations are little affected by post-depositional processes (Iizuka et al., 2018). Even for nitrate, the photochemical reaction is negligible in the surface at this site (Iizuka et al., 2018).

We selected 1973–1975 for the period of anthropogenic sulfate maximum ("1970s") and 2010–2012 for the period after regulation of sulfur emission ("2010s") (Figure 1). For the 1970s, we analyzed the chemical components in 30 ice sections dated as covering 19th December 1973–25th May 1975. For the 2010s, we measured 37 ice sections covering 9th May 2010–29th May 2012. Thus, we measured a total of 67 sections covering 42 months (Figure 1).

2.2. SEM/EDS Measurement

For the component analyses, we pulverize about 2 g of the ice (or snow) from a sample and sublimate it on a Teflon filter with a pore size of 0.4 μm (Advantec, H040A013A) at −50°C using clean, dry air (as in Iizuka et al., 2009). All filters are coated with platinum to a thickness of 10 nm using magnetron sputtering for 30 s (Vacuum Device, MSP-10). We then analyze the 67 filter samples using a SEM/EDS system (JEOL, JSM-6360LV/JED2201). Each

filter yielded several hundred nonvolatile particles exceeding 0.4-μm diameter (Figure S1 in Supporting Information S1). For each such particle, we estimate the surface area (μm^2). Using SEM-EDS at 20 keV, we determine the atomic mass percentages of O, Si, Al, S, Cl, Na, Mg, K, and Ca in the particles (Figure S1 in Supporting Information S1). In total, 12,325 particles were analyzed, giving an average of 184 particles per filter. Originally, a given filter would have 400–500 particles after the sublimation. From these particles, we randomly sample 184, which in the case of 500 to sample from, gives a tolerant error of 5.7% with confidence level of 95%. We do not analyze levels of C and N due to inaccuracies with light elements.

To determine the sulfate components, we use the sublimation_EDS method (Iizuka et al., 2009; Iizuka, Uemura, et al., 2012). This method identifies the nonvolatile particles and separates the nonvolatiles into soluble and insoluble components. Particles containing Si are assumed to have silicate material. We also assume that all S in the nonvolatile particles are from soluble material (Figure S2 in Supporting Information S1) such as sulfate salts (Iizuka, Uemura, et al., 2012). Dry air ventilation removes gas-phase compounds such as HCl and HNO_3, and remnant solution (H_2SO_4) becomes undetectable under the SEM environment and measurement procedure. Unlike previous studies (Iizuka et al., 2009; Iizuka, Uemura, et al., 2012), we distinguish the sulfuric acid in liquid droplets (SO_4^{2-}) from gaseous H_2SO_4 (i.e., H_2SO_4(g)).

After considering the possible remaining compounds, we assume that Na and S in a given particle came from Na_2SO_4, whereas Ca and S are assumed to come from $CaSO_4$ (Figure S1 in Supporting Information S1). (A similar assumption has been used in other studies (Chi et al., 2015; Hara et al., 2014).) If S is found in particles without Na or Ca, we regard the S-containing particles as ammonium sulfate salt ($(NH_4)_2SO_4$), which is now common in the Arctic atmosphere (Park et al., 2004). We ran tests on ice sections from spring 1974, summer 2003, and winter 2011. The nonvolatile particles were collected by the sublimation method, whereas the insoluble particles were collected by filtration of the melted sample from the same depth, with both groups examined with SEM/EDS (Iizuka et al., 2009). For example, in the case of summer 2003, we measured 200 nonvolatile and 318 insoluble particles. For this summer, more than 99% of the total insoluble particles contain Si (Figure S2b in Supporting Information S1, right side, yellow bar), suggesting that the particles containing Si are insoluble materials such as silicate. For S, we detected S in 14% of the nonvolatile and none of the insoluble particles (light blue bar). The Cl results show a similar trend (green bar). This overall pattern repeats in the other filters (spring 1974, winter 2011). These results suggest that particles containing either S or Cl are soluble materials (likely sulfate or chloride) and thus reconfirm the effectiveness of the above scheme for the Greenland ice core.

2.3. Mass Weights of Silicate and Sulfate Salt

For particle diameters over 0.4 μm, we calculate mass weights of silicate and sulfate salt using the mass ratio of Si and S in a particle, and the particle surface area (Iizuka, Ohno, et al., 2016; Iizuka, Tsuchimoto, et al., 2012). By summing the mass weights of silicate and sulfate salts in each particle, we obtain the total mass weights of silicate and sulfate salts. In a given particle, the mass weight of Na_2SO_4 is assumed from the lower mole-equivalent weight between Na and S. The same holds for $CaSO_4$ using Ca and S. For example, if the mass weights of sodium and sulfur are expressed as [Na] and [S], then the mass weights of Na_2SO_4 is $[Na_2SO_4] = [Na]$ if $[Na] < [S]$ (eq); otherwise, $[Na_2SO_4] = [S]$. For the mass weights of $(NH_4)_2SO_4$, we assume that the sulfate mass weight in the case of S was found having neither Na nor Ca. Thus, the mass weights of $(NH_4)_2SO_4$ is $[(NH_4)_2SO_4] = [S]$ (eq).

Following our previous work (Iizuka, Uemura, et al., 2012), a particle containing Si is assumed to be silicate dust. Then, to estimate the total mineral dust mass, we multiply the Si mass by 0.28^{-1}, due to the average abundance of silicon in Earth's crust being 28%. In a similar manner, S-containing particles in the nonvolatile particles can be regarded as large solid sulfate salts exceeding 0.4-μm diameter. Thus, to estimate the sulfate mass, the S mass is multiplied by 96.07×32.065^{-1}, the ratio of molecular weights of SO_4^{2-} and S. Any liquid inclusions such as SO_4^{2-} larger than 0.4 μm diameter cannot be detected as particulate residues by the sublimation method as explained in the next section.

The uncertainty of the number ratio is based on the assumption that the errors follow the Poisson distribution law. For example, the uncertainty of the number ratio of sulfate salt to mineral dust for the 2010s is 0.10 ± 0.07 and for the 1970s is 0.08 ± 0.03. Details of the method are in (Iizuka, Tsuchimoto, et al., 2012). For the mass ratio, the uncertainty is based on the coefficient of variation (CV) for each atomicity ratio and the spherical approximation. For the atomic ratio, we used 0.40 as the CV (Iizuka, Tsuchimoto, et al., 2012). For the spherical

approximation, the calculated uncertainty for 95% of the particles is below 0.20 (Iizuka, Uemura, et al., 2012). The average uncertainty and the standard deviation of the mass ratio of sulfate salt to mineral dust is 0.22 ± 0.02 in the 2010s and 0.22 ± 0.01 in the 1970s. These uncertainty values are slightly higher than those from the ratio of sulfate ion and dust concentrations measured using ion chromatography and coulter counter (i.e., 0.10 and 0.15, respectively). Details of this CV method are in (Iizuka, Tsuchimoto, et al., 2012).

2.4. Evaluation of Sulfuric Acid Droplets Larger Than 0.4 μm

We used the sublimation method on a winter 1974 sample to estimate whether a significant number of sulfuric acid droplets larger than 0.4 μm were deposited at SE-Dome. In this case, we put the sample on a Ni mesh (DN200 mesh, Okenshoji) instead of the Teflon filter. After sublimation on the Ni mesh, any residue of sulfuric acid droplets would react to $NiSO_4$ on the mesh, showing up in the SEM/EDS measurement as an increase in mass proportion of S-containing particles. We found the mass proportion of S-containing particles in relation to total particles to be 0.05. This value is not larger than the value of 0.12 from the same ice sample on the Teflon filter, and is also within the range 0.09 ± 0.06 that was found for the 1970s. This result indicates that if sulfuric acid droplets larger than 0.4 μm are deposited, then they must be too few in number to significantly contribute to the sulfur signal. In agreement with this test, micro-Raman measurements of the nonvolatile particles (>0.6 μm) on a Ni plate in the SE-Dome ice cores never detected the $NiSO_4$ peak of 987 cm^{-1}.

During the sublimation at −50°C, all sulfate salts considered here are solid, whereas sulfuric acid is liquid. In particular, the eutectic points of $(NH_4)_2SO_4$, Na_2SO_4 $10H_2O$, $CaSO_4$ $2H_2O$, and H_2SO_4 are −19.0, −1.3, −0.05, and −56.4°C (at 34.6%), respectively. Thus, whereas the liquid sulfuric acid might spread out and bind with the Teflon filter during the sublimation step and thus be lost from the SEM image, the solid sulfate should hardly shrink. Also, we assume that the size and chemical forms of sulfate salts in the ice core reconstruct their state in surface snow just after wet deposition. On the other hand, our analyses do not reveal their prior states, such as the size and compounds during emission and atmospheric transport.

Solid sulfate salts here may be relatively unaffected by post-depositional effects that can alter other impurities in inland ice sheets. In particular, solid sulfate salts are found within ice grains (Ohno et al., 2005), suggesting that they are stably isolated from the surrounded ice matrix. Furthermore, the SE-Dome region's high accumulation rate should greatly reduce post-depositional effects. For example, here even NO_3^- is well preserved (Iizuka et al., 2018), suggesting the reaction of sulfate salt formation of $NaNO_3 + H_2SO_4 \rightarrow Na_2SO_4 + HNO_3$ in snow is not likely to occur. On the other hand, liquid sulfuric acid may aggregate in snowpack or during sublimation. Sulfuric acid is likely to exist at the grain boundary of ice (or surface of snow particle), forming a liquid layer with SO_4^{2-} (Mulvaney et al., 1988). Such SO_4^{2-} can coalesce in snowpack or during sublimation, resulting in larger droplets. For this reason, we checked for sulfuric acid droplets larger than 0.4 μm on the Ni mesh.

2.5. Aerosol Model Simulations for Sulfate Deposition Fluxes

To estimate deposition fluxes of sulfate aerosols originating from anthropogenic and natural (biogenic) sources, we used Coupled Model Intercomparison Project 6 (CMIP6) historical simulation data calculated by the Meteorological Research Institute Earth System Model version 2 (MRI-ESM2.0 (Oshima et al., 2020; Yukimoto et al., 2019)). MRI-ESM2.0 consists of four main parts: an atmospheric general circulation model with land processes (MRI-AGCM3.5), an ocean-sea-ice general circulation model (OGCM), an aerosol chemical transport model, and an atmospheric chemistry model. The horizontal resolution of the atmospheric general circulation model (GCM), aerosol, and chemistry sub-models are about 120, 180, and 280 km, respectively, all with the same 80 vertical layers from the surface to the model top at 0.01 hPa.

The aerosol model tracks non-sea-salt sulfate, black carbon, organic carbon, sea salt, mineral dust, and aerosol precursor gases (e.g., sulfur dioxide and dimethylsulfide). The size distributions of sea salt and mineral dust have 10 discrete bins. The other aerosols are represented by lognormal size distributions and the size-distribution parameters assumed in the model are described elsewhere (Yukimoto et al., 2019). Sulfur species originating from anthropogenic sources are separated from natural sources. Emissions of mineral dust, sea salt, and sulfur species originating from a natural source (e.g., dimethylsulfide from the ocean) are interactively calculated in the model. Sulfate aerosols form via gas- and aqueous-phase reactions by oxidants arising from atmospheric ozone chemistry.

We ran 10 ensemble members of the historical simulations for 1850–2014. Their initial states came from the pre-industrial control experiment that started from the final state of the 1,000-year spin-up run with the 1,850 condition. The CMIP6 forcing data set includes greenhouse gas concentrations (Meinshausen et al., 2017), anthropogenic and open biomass burning emissions of short-lived climate forcers (Hoesly et al., 2018; van Marle et al., 2017), and volcanic stratospheric aerosol data (Thomason et al., 2018). Further details of the CMIP6 historical simulations by MRI-ESM2.0 are described in Yukimoto et al. (2019).

3. Data

To compare the mass weights of silicate and sulfate salt by the SEM/EDS measurements, we use published ice core data of oxygen isotope ratio, seasonal accumulation rates (Furukawa et al., 2017), ion concentrations and fluxes (Iizuka et al., 2018), as well as dust concentrations and fluxes (Amino et al., 2020). For a summary of the data on the oxygen isotope ratio as well as the ion and dust concentrations, see the supplemental data. The seasonal accumulation rate, ion concentration, and dust concentration are calculated by averaging the raw data (Table S1 in Supporting Information S1). The seasonal fluxes of sulfate ion and dust are calculated from the sulfate ion and dust concentrations, together with the seasonal accumulation rates in the SE-Dome ice core.

4. Results and Discussion

4.1. Mass Ratios of Sulfate Salt and Insoluble Dust on Single Particles

For the mass ratios, we examined all the particles on each filter sample, finding about one fourth the mass being Si (0.25 ± 0.05 for the 1970s, 0.25 ± 0.11 for the 2010s) and about one tenth the mass being S (0.09 ± 0.06 for the 1970s, 0.09 ± 0.07 for the 2010s). Figure 2a shows that the mass fraction of silicon (Si) and sulfur (S) in each particle remains essentially the same between the two periods. Therefore, the S/Si mass ratio $R_{s/si}$ (red, Figure 2b) hardly changed between the 1970s (0.31 ± 0.22) and the 2010s (0.37 ± 0.42). (As described in the methods section, $R_{s/si}$ is adjusted for Si abundance in dust and S fraction in sulfate ion to compare directly to $R_{SO_4/dust}$). However, the 1970s have higher sulfate ion concentrations and lower dust concentrations compared to those for the 2010s (Figure S3 in Supporting Information S1). Thus, the concentration ratio of sulfate ion to dust $R_{SO_4/dust}$ is higher during the 1970s (2.53 ± 0.91) than that during the 2010s (0.92 ± 0.78) (purple, Figure 2b).

4.2. Separation of Sulfate Ion Concentration Into Large Sulfate Salt and Small Sulfur Compounds

Sulfate ion concentrations here substantially decrease from 59.5 ± 18.3 μg kg^{-1} in the 1970s to 23.2 ± 15.9 μg kg^{-1} in the 2010s (light blue, Figure S3b in Supporting Information S1). This factor of two decrease roughly equals the decrease in anthropogenic SO_2 emissions flux between these periods (Figure 8 of Iizuka et al., 2018). This finding is consistent with measurements elsewhere in Greenland. For example, sulfate fluxes in Greenland ice cores tend to be higher near anthropogenic sources and coastal areas (biogenic sulfate), but at a given location, the sulfate fluxes are higher in the 1970s than in the post-2000 period, which is a general trend seen in all ice cores (e.g., Bauer et al., 2020; Fischer et al., 1998).

This link to anthropogenic SO_2 emissions flux is also supported by the seasonal variations in the sulfate ion profiles. Indeed, while the sulfate profile during the 1970s shows a constantly high sulfate concentration without clear seasonality (Figure S3b in Supporting Information S1), the sulfate profile during the 2010s shows a seasonal fluctuation with spring–summer maximum (Figure S3b in Supporting Information S1). In contrast, the average dust concentration during the 1970s (25.0 ± 7.04 μg kg^{-1}) is slightly lower than that of the 2010s (34.4 ± 22.2 μg kg^{-1}) (brown circles, Figure S3b in Supporting Information S1). The higher dust levels in the 2010s likely arise from an increase in soil exposure due to the decrease in seasonal (summer–autumn) snow cover (Amino et al., 2020).

To better understand possible changes between the two periods, we divide the sulfate ion concentration into two size categories: (a) sulfate salt on particles of diameter over 0.4 μm and (b) sulfate salt on particles of diameter less than 0.4 μm. The latter category includes small sulfuric acid droplets. As a first step, we examine the mass ratios. The sulfate measured for $R_{s/si}$ is on the particles over 0.4 μm. The $R_{SO_4/dust}$ is the mass ratio of dissolved sulfate compounds measured with the ion chromatography to the total insoluble dust measured with the coulter counter (Figure 1). The dissolved sulfate concentrations are the sum of the liquid sulfuric acid and the solid

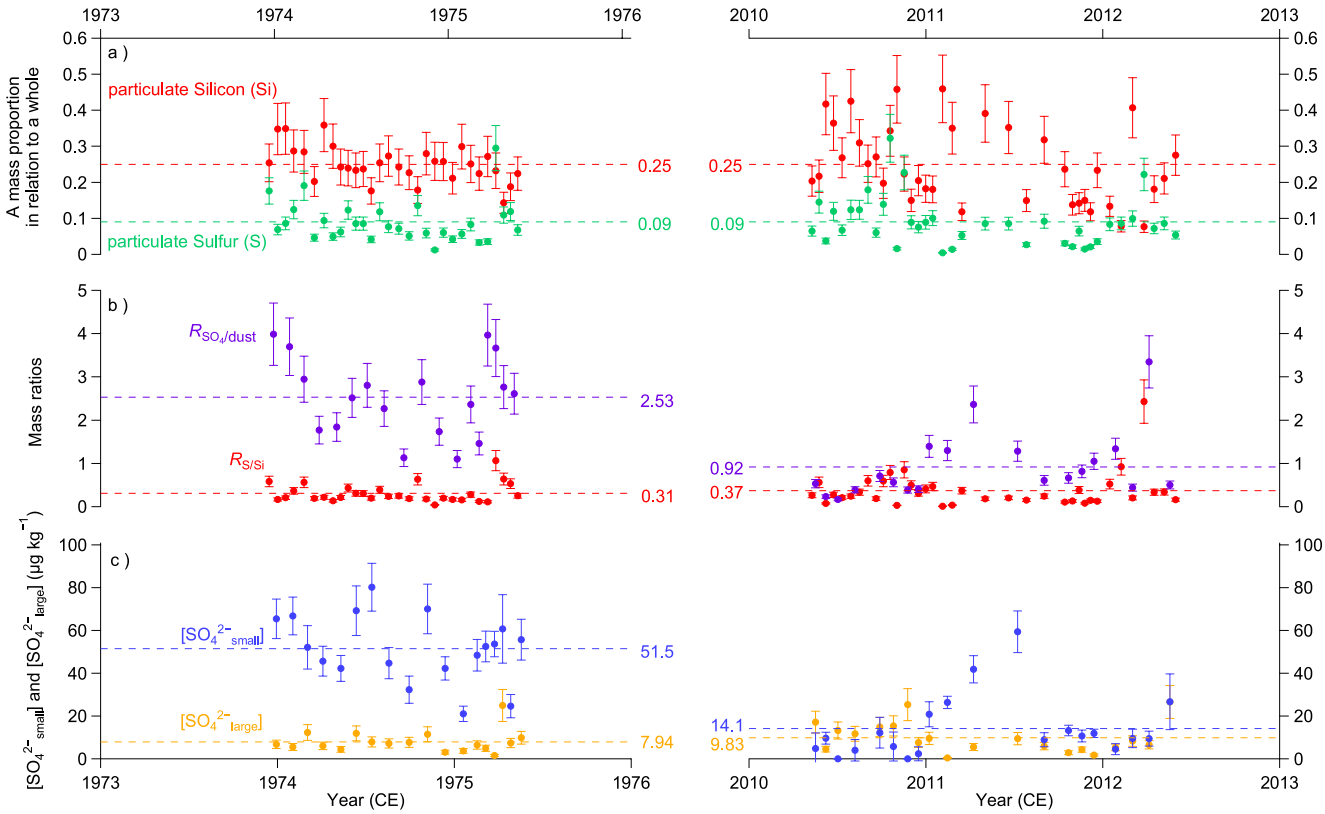

Figure 2. Silicon (Si), sulfur (S), SO_4^{2-}, and dust levels in examined particles from the 1970s and 2010s. (a) Mass of silicon (brown) and sulfur (green) divided by the particle mass from EDS measurements. Each data point is from measurements of fraction C (Figure 1) on about 184 particles on a given filter. Dotted lines are average values. (b) Mass ratio of sulfate ion to dust concentrations ($R_{SO_4/dust}$; purple) from the data of Figure S3b in Supporting Information S1 and from measurements of fraction B (Figure 1). The mass ratios ($R_{s/si}$; red) of sulfur (S) and silicon (Si) are from plot (a) above. The purple includes both small and large sulfate, whereas the red includes only large sulfate. (c) $[SO_4^{2-}{}_{small}]$ (blue) and $[SO_4^{2-}{}_{large}]$ (orange) concentrations (μg kg^{-1}) from the two mass ratios in Figure 2b. $[SO_4^{2-}{}_{large}]$ is the sulfate salt concentration of large particles (larger than 0.4 μm), whereas $[SO_4^{2-}{}_{small}]$ is from both small liquid sulfuric acid droplets and sulfate salt particles (smaller than 0.4 μm).

sulfate salts of any size. The Si obtained by the sublimation method is assumed to be the same as the dust by the dissolved method, as they both are insoluble materials. Most of the $R_{SO_4/dust}$ values are higher than the $R_{s/si}$ values in the 1970s (Figure 2b), which indicates that the sulfur compounds existed mainly as sulfuric acid droplets and sulfate salt smaller than 0.4 μm. In the 2010s, the $R_{s/si}$ values are close to those of $R_{SO_4/dust}$.

To calculate $[SO_4^{2-}{}_{large}]$, the concentrations (μg kg^{-1}) of sulfate salts larger than 0.4 μm, we use

$$\left[SO_4^{2-}{}_{large}\right] = \frac{R_{S/Si}}{R_{SO_4/dust}} \left[SO_4^{2-}\right] \quad (1)$$

where $[SO_4^{2-}]$ is the total ion concentration. For the $[SO_4^{2-}{}_{small}]$, which is the concentration of sulfuric acid in droplets and sulfate salt smaller than 0.4 μm, we subtract the large contribution from the total:

$$\left[SO_4^{2-}{}_{small}\right] = \left[SO_4^{2-}\right] - \left[SO_4^{2-}{}_{large}\right] \quad (2)$$

In the rare case that $R_{s/si}$ exceeds $R_{SO_4/dust}$, we assume that all sulfate ions were in the large sulfate salt, that is, $[SO_4^{2-}{}_{large}] = [SO_4^{2-}]$ and $[SO_4^{2-}{}_{small}] = 0$.

The average $[SO_4^{2-}{}_{small}]$ greatly decrease from 51.5 ± 15.9 μg kg^{-1} in the 1970s to 14.1 ± 14.8 μg kg^{-1} in the 2010s (Figure 2c). In contrast, $[SO_4^{2-}{}_{large}]$ hardly changes between the periods (Figure 2c, Table S2 in Supporting Information S1). Given that the 1970s is a period of high anthropogenic SO_2 emission, the high $[SO_4^{2-}{}_{small}]$ likely originated from anthropogenic SO_2. The relatively low and nearly equal $[SO_4^{2-}{}_{large}]$ concentrations for the 1970s

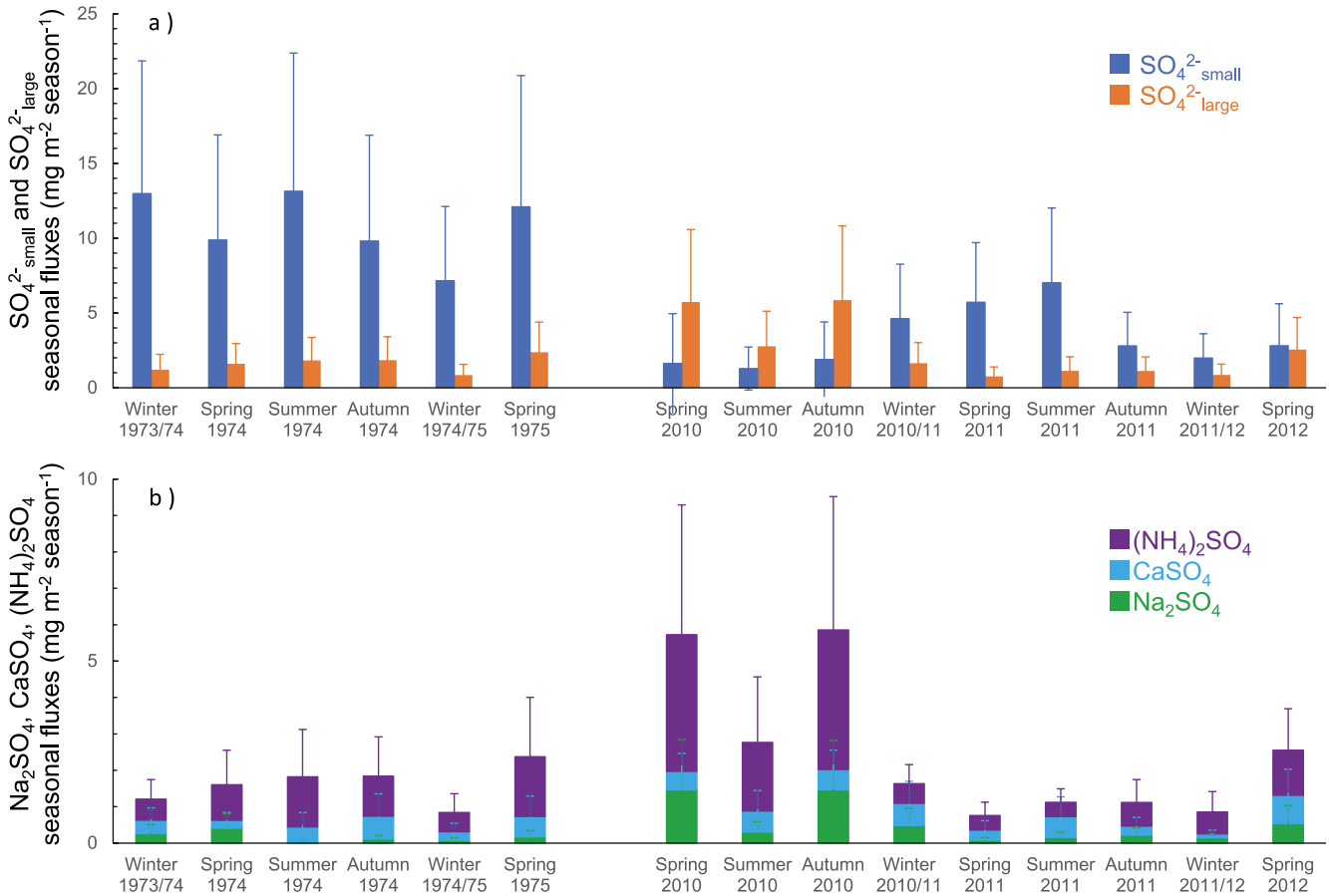

Figure 3. Seasonal flux of sulfate compounds (mg m^{-2} season^{-1}) from the 1970s (left), and from the 2010s (right). (a) $SO_{4\ small}^{2-}$ (blue) and $SO_{4\ large}^{2-}$ (orange) fluxes from Figure 2c. The sum of the $SO_{4\ small}^{2-}$ and $SO_{4\ large}^{2-}$ fluxes equals the sulfate ion flux. (b) Na_2SO_4 (green), $CaSO_4$ (light blue), and $(NH_4)_2SO_4$ (purple) fluxes. The sum of these fluxes equals the $SO_{4\ large}^{2-}$ flux in panel (a) (orange).

and 2010s implies that anthropogenic sulfuric acid, which has significantly decreased since the 1970s, is not likely to have produced these large sulfate salt particles during transport processes in the atmosphere.

4.3. Seasonal Flux of Large Sulfate Salt and Small Sulfur Compounds

The seasonal fluxes of $SO_{4\ large}^{2-}$ and $SO_{4\ small}^{2-}$ are calculated from the [$SO_{4\ large}^{2-}$] and [$SO_{4\ small}^{2-}$], as well as from the seasonal accumulation rates in the SE-Dome ice core (Furukawa et al., 2017). Throughout this study, a season is a 3-month period: March–May for spring, June–August for summer, September–November for fall, and December–next February for winter. Averaged over the periods, the seasonal flux of $SO_{4\ small}^{2-}$ during the 1970s is 10.8 ± 2.32 mg m^{-2} season^{-1}, about three times that during the 2010s (3.30 ± 2.02 mg m^{-2} season^{-1}) (Table S2 in Supporting Information S1). On the other hand, the seasonal flux of $SO_{4\ large}^{2-}$ during the 1970s (1.62 ± 0.54 mg m^{-2} season^{-1}) is slightly lower than that during the 2010s (2.49 ± 2.00 mg m^{-2} season^{-1}).

Considering the seasonal trends in Figure 3a, in winter the $SO_{4\ small}^{2-}$ fractions exceed those of $SO_{4\ large}^{2-}$, consistent with our argument that they have an anthropogenic source. Also, some seasonality for $SO_{4\ small}^{2-}$ is apparent between 2011 and 2012, showing a higher summer flux, but the 1970s results in Figure 3c show no seasonality, suggesting anthropogenic sulfuric acid may contribute to winter flux in the 1970s. Some insight into the chemical processes comes from examining the anion and cation levels. Table S1 in Supporting Information S1 shows that the [SO_4^{2-}] levels are less than those of the total cations during all seasons in the 2010s. On the other hand, in the 1970s, the [SO_4^{2-}] levels exceed those of the cations during most seasons (Table S1 in Supporting

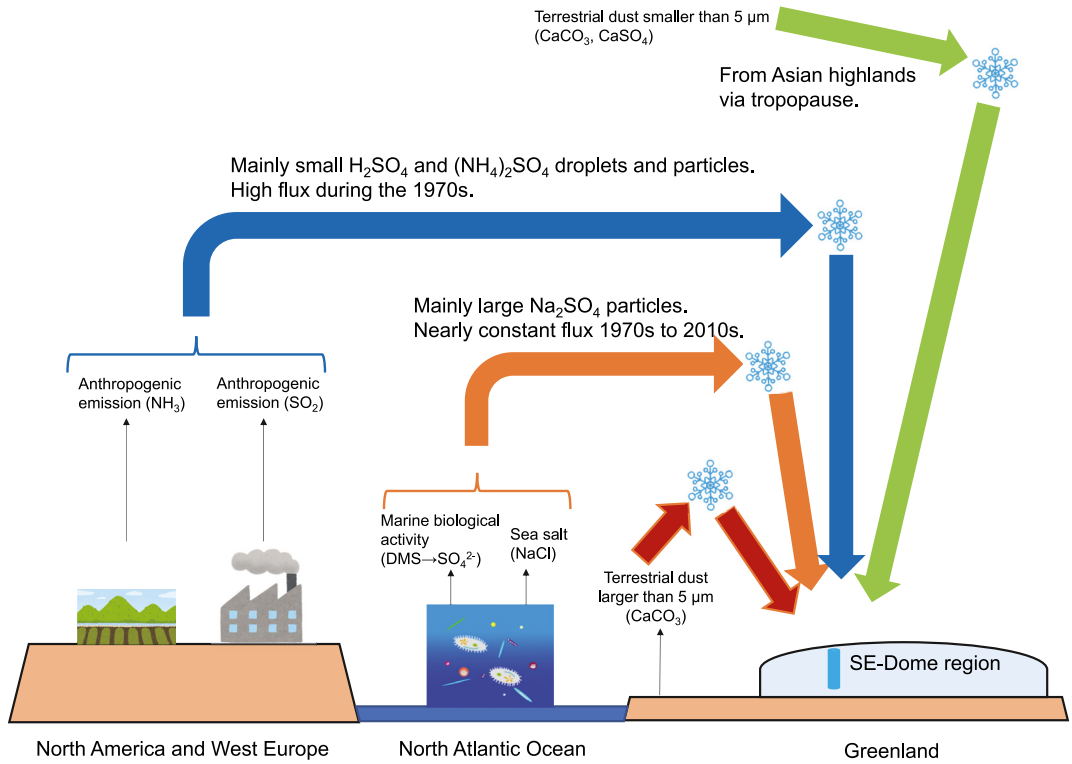

Figure 4. Sulfate sources, transport, and deposition to the SE-Dome ice core. The near sulfate sources are from natural marine biological activity in the North Atlantic, which is also the source of sea salt. This region is the likely source of large Na_2SO_4 particles. Further sulfate sources are mainly from North America and Western Europe, due largely to oxidation of SO_2 from anthropogenic emissions. These regions are the likely source of small SO_4^{2-} droplets and $(NH_4)_2SO_4$ particles. The $CaSO_4$ sources are likely the Asian highlands and coastal Greenland. Snow crystal symbol indicates wet deposition. Not shown is the contribution from volcanic eruptions, which was insignificant during the study periods.

Information S1), which is consistent with the 1970s having a larger aerosol flux of non-neutralized sulfuric acid than the 2010s. Thus, the high fraction of sulfate flux from $SO_{4\ small}^{2-}$ in the 1970s is likely due to non-neutralized sulfuric acid.

Southeastern Greenland is thousands of kilometers from the nearest land emission areas of North America and West Europe, the likely sources of the small aerosols (Sirois & Barrie, 1999). These small aerosols also provide the largest sulfur flux to the ice core, suggesting that the anthropogenic sulfur particles were relatively small in the atmosphere and if they were CCN, then their combination of being relatively small and numerous would imply that they had a relatively large radiative forcing. Hence, understanding the small sulfate particles is important for the precise reconstruction of aerosol radiative forcing during the 1970s and how the sulfate particles can cool the Arctic region.

4.4. Transport of Sulfate, Dust, and Sea-Salt Aerosols to SE-Dome

The Na_2SO_4, $CaSO_4$, and $(NH_4)_2SO_4$ salts form by sulfatisation of SO_4^{2-} during their transport through the atmosphere. Na_2SO_4 and $CaSO_4$ form by SO_4^{2-} sulfatisation on the surface of sea salt (NaCl) and dust ($CaCO_3$) particles, respectively. The sea salt to the SE-Dome region largely comes from the North Atlantic Ocean (Iizuka et al., 2018), whereas the Ca-related dust has many potential source areas from near land area in coastal Greenland to distant Asian highlands (Amino et al., 2020). Gypsum ($CaSO_4{\cdot}2H_2O$) in terrestrial dust also travels far, from the Asian highlands (green arrow in Figure 4) to the SE-Dome area (Miyamoto et al., 2022). On the other hand, $(NH_4)_2SO_4$ salts form by condensation of SO_2 and NH_3 gases as well as by aqueous-phase reactions of SO_2 and NH_3 in water drops. An insignificant difference of condensational growth by the SO_2 and NH_3 reactions between the 1970s and 2010s is likely the main reason for the insignificant difference of large sulfate salt fluxes between these periods.

To better understand the large sulfate salt flux, we divide the $SO_{4\ large}^{2-}$ seasonal fluxes into Na_2SO_4, $CaSO_4$, and $(NH_4)_2SO_4$ fluxes as in Figure 3b. For both periods, the dominant component for $SO_{4\ large}^{2-}$ is the $(NH_4)_2SO_4$ flux. In the 1970s, it is 1.03 ± 0.44 mg m^{-2} $season^{-1}$ (64% of total $SO_{4\ large}^{2-}$), and in the 2010s it is 1.48 ± 1.40 mg m^{-2} $season^{-1}$ (59% in total $SO_{4\ large}^{2-}$). Similarly, the $CaSO_4$ (0.41–0.47 mg m^{-2} $season^{-1}$) are nearly the same in both periods. The $SO_{4\ large}^{2-}$ flux increased by 154% from the 1970s (1.62 mg m^{-2} $season^{-1}$) to the 2010s (2.49 mg m^{-2} $season^{-1}$), driven mainly by an increase in Na_2SO_4 flux.

Between the two periods, the Na_2SO_4 flux increased from 0.18 to 0.54 mg m^{-2} $season^{-1}$, in spite of the $[Na^+]$ and $[SO_4^{2-}]$ decreasing from the 1970s to the 2010s (Table S1 in Supporting Information S1). Thus, the 2010s has more sulfatization of sea salt. A possible reason for this increase is a shift in the main source of $[Na^+]$ and $[SO_4^{2-}]$ between the 1970s and 2010s (Figure 4). Specifically, the SO_2 origin shifts from mainly anthropogenic in the 1970s to mainly natural in the 2010s, which is a shift from North America and West Europe to the North Atlantic Ocean. The former regions are also a source of NH_3, leading to formation of $(NH_4)_2SO_4$, the latter is also source of sea salt (Seguin et al., 2011), leading to formation of Na_2SO_4. Between the 1970s and 2010s, the natural SO_2 emission in the North Atlantic may have increased due to higher chlorophyll and therefore higher dimethylsulfide masses. (Chlorophyll increased from 1997 to 2016 (von Schuckmann et al., 2018), and some proxies showed the chlorophyll mass during 1970s being lower than that during around 2000 (Boyce et al., 2010; Osman et al., 2019)) As sulfate during the 1970s arrived from a different pathway than that of sea salt (Figure 4), sea-salt modification to sodium sulfate was less likely to occur.

The $[Ca^{2+}]$ in the 1970s (0.22 mg m^{-2} $season^{-1}$) is about 60% of that in the 2010s (0.36 mg m^{-2} $season^{-1}$) (Table S1 in Supporting Information S1). In both periods, $[Ca^{2+}]$ is lower than $[SO_4^{2-}]$, implying that $CaSO_4$ should form if Ca^{2+} and SO_4^{2-} were contacting each other. However, the $CaSO_4$ flux (0.41–0.47 mg m^{-2} $season^{-1}$) is about the same in both periods, suggesting that not all Ca^{2+} reacted with SO_4^{2-}during the transport. A possible reason is a difference in source regions (Figure 4). First, the local dust from Greenland's coast is a source of Ca^{2+} (Amino et al., 2020), which is probably a different pathway than the anthropogenic sulfate during the 1970s. Second, an earlier study found that anthropogenic sulfate (H_2SO_4) from China would react with $CaCO_3$, forming $CaSO_4$ before arriving in Japan (Takahashi et al., 2009). If we apply that observation here, then a higher $CaCO_3$ contribution to Greenland in the 1970s may be due to there being lower SO_2 emissions in China back then. On the other hand, the anthropogenic SO_2 flux from North America and West Europe was high at this time. If the Asian $CaCO_3$ were to react with anthropogenic sulfate (H_2SO_4) from North America and West Europe, then the $CaSO_4$ flux should be higher during the 1970s than that during the 2010s. Thus, the constant $CaSO_4$ flux suggests (a) a different pathway between Asian dust ($CaCO_3$) and anthropogenic SO_2 from North America and West Europe (Figure 4), and (b) a smaller contribution from Asian dust ($CaCO_3$ and $CaSO_4$) to the total dust in the SE-Dome ice core. This argument suggests that sulfate during the 1970s was transported via a pathway differing from that of dust (Figure 4), and thus the dust modification to calcium sulfate was not likely to occur.

4.5. Aerosol Model Simulations of Sulfate Deposition Fluxes

We ran the MRI-ESM2.0 model to simulate the contributions, both anthropogenic and natural, to the deposited sulfate flux from 1950 to 2014 in the SE-Dome region. In Figure 5, we compare these simulated fluxes to the sulfate ion flux (1960–2014) in the SE-Dome ice core (Iizuka et al., 2018). The agreement is good except in years of large volcanic sulfate contributions such as in 2014 (from Bardarbunga, Iceland). The simulated sulfate flux of anthropogenic origin during 1973–1975 (42.6 ± 25.4 mg m^{-2} yr^{-1}) is four times higher than that during 2010–2012 (10.7 ± 2.74 mg m^{-2} yr^{-1}), agreeing closely to the flux change of $SO_{4\ small}^{2-}$ from 43.36 ± 9.30 to 13.20 ± 8.06 mg m^{-2} yr^{-1} found here for these periods.

The anthropogenic sulfate in the SE-Dome ice core mainly comes from emitted SO_2 gas from North America and Europe. These regions emit relatively little large sea salt and dust particles compared to their emissions of cationic materials from anthropogenic gas NH_3 and small anthropogenic particles (e.g., fly ash). Thus, the simulations support our argument that the anthropogenic SO_2 from these regions is likely to form small SO_4^{2-} liquid droplets and small sulfate salt particles due to condensation of H_2SO_4 on small particles and aqueous-phase reactions by SO_2 on aerosol-originated cloud droplets.

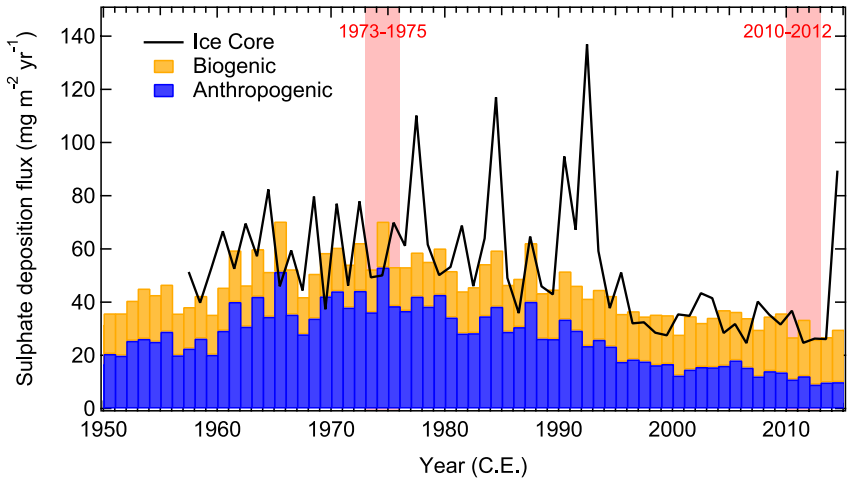

Figure 5. Observed and simulated annual mean sulfate deposition flux. Simulated sulfate fluxes originating from anthropogenic and natural (biogenic) sources are shown in blue and orange bars, respectively. The model results are ensemble-mean of 10 members of the historical simulations by MRI-ESM2.0. The black line is the observed sulfate flux from the SE-Dome ice core. The simulations do not include deposited volcanic sulfate, but they do include effects of the volcanic aerosols on climate. The pink bars mark the periods of measured fluxes of $SO_{4\ small}^{2-}$ and $SO_{4\ large}^{2-}$ from the ice core.

As we also found here, the simulations show that the sulfate flux of natural origin during the 1970s is similar as that during the 2010s (16.1 ± 4.66 vs. 18.0 ± 5.56 mg m^{-2} yr^{-1}). Natural sulfate in the SE-Dome ice core mainly comes from emitted dimethylsulfide from the North Atlantic and then oxidized to SO_2 gas. Having the SO_2 gas and sea-salt particles in the same air masses during transport would promote the formation of large Na_2SO_4 particles. The similar $SO_{4\ large}^{2-}$ fluxes during the 1970s and 2010s (5.68 ± 2.16 vs. 9.96 ± 8.00 mg m^{-2} yr^{-1}) are consistent with the simulated natural sulfate fluxes for those periods, although sulfate production from biogenic SO_2 would contribute to both the $SO_{4\ small}^{2-}$ and the $SO_{4\ large}^{2-}$ fluxes.

The model simulations show increases in the anthropogenic sulfate fluxes in 1960–1990, followed by a gradual decreasing trend of the fluxes; however, the natural sulfate fluxes are nearly constant throughout the entire period (Figure 5). The two periods of 1973–1975 and 2010–2012 correspond to the largest and smallest anthropogenic contributions, respectively, supporting our choice of these periods. The model results show larger contributions of natural origin than anthropogenic origin since around 2000 (Figure 5) and the relative contribution of natural origin will continue to increase over the near-term future due to further reductions in anthropogenic SO_2 emissions in future scenarios (Gidden et al., 2019). Although the measurement techniques used in this study could not distinguish biogenic from anthropogenic sulfate, our results suggest the importance of resolving both particle size and origin (anthropogenic vs. biogenic) of sulfate aerosols in the ice core measurements, which could be partly achieved by incorporating sulfur isotope measurements into future studies.

4.6. Implications of Sulfate Aerosols During the 1970s

Our main finding is that the flux of the small sulfur particles is higher during the 1970s than that during the 2010s, whereas the larger sulfate particle flux stayed essentially unchanged. These particles are relevant to the aerosol-cloud interaction that, according to models, cooled the Arctic region in the 1970s (Chylek et al., 2016). However, observational knowledge of past aerosol size distributions has been insufficient, resulting in large uncertainties in estimates of aerosol climate effects. Global aerosol-climate models use microphysical processes to determine the particle size distribution (Mann et al., 2014), with some models showing that the spatial distributions of aerosols and their climatic effects are highly sensitive to the treatment of the aerosol size distribution (Mann et al., 2014; Matsui et al., 2018; Reddington et al., 2011).

In this study, we have taken a step toward providing measurements of past aerosol sizes preserved in an ice core. We found a higher fraction of $SO_{4\ small}^{2-}$ to the total sulfate flux during the 1970s than in the 2010s, an important finding for constraining models and their estimates of climate effects for the Arctic. In particular, because the

smaller aerosols imply a higher number concentration of particles or droplets than larger aerosols with the same aerosol mass, the amount of scattered radiation would be larger, particularly if the particles acted as CCN. The results here suggest that there were more CCNs during the 1970s than aerosol mass estimation. Thus, our findings may help to improve understanding of the aerosol-cloud interactions for the modeling of past climates (Eyring et al., 2016; Gillett et al., 2016).

4.7. Future Implications

Looking toward the future, continued reductions in anthropogenic SO_2 may continue to accelerate global warming (Chylek et al., 2016; Gillett et al., 2016). Moreover, in the Arctic, polar amplification of global warming will increase the sea surface temperature, which is predicted to increase the marine biological activity and dimethylsulfide emission (Mahmood et al., 2019). Such an increase may lead to an increase in new particle formation over the ocean, which, through increased CCN production, produces higher albedos in the marine boundary layer clouds, causing a cooling feedback (Kerminen et al., 2018). Our results suggest that the SO_2 from dimethylsulfide is likely to form large sulfate salts (e.g., Na_2SO_4) during transport to highlands over the Greenland ice sheet, suggesting that the relationship between sulfate and CCN may differ between marine and highlands regions.

Also, according to Hattori et al. (2021), the triple oxygen isotopic compositions ($\Delta^{17}O$) of sulfate have increased since the 1980s, which indicates greater importance of in-cloud sulfate production. In-cloud sulfate production is a potentially important source of accumulation mode-sized CCN due to both the growth of activated Aitken particles and the higher coalescence efficiency of processed particles (Roelofs et al., 2006). Also, any differences in oxidation pathways for anthropogenic and biogenic aerosols (e.g., acidity) could have significant effects on CCN and precipitation that are not currently captured in the models. However, the relationship between SO_2 from dimethylsulfide in the marine area and the flux of sulfate salts to the ice sheet is complex, and may also be influenced by precipitation rates (Mahmood et al., 2019). As such, further studies are required to predict CCN-based aerosol-cloud interactions in the future.

5. Conclusions

We have analyzed mass ratios of sulfate salt and insoluble dust on single particles in the high-resolution ice core from southeastern Greenland between the anthropogenic sulfate maximum (1973–1975) and after sulfur emissions control (2010–2012). Then, we have separated sulfate ion concentration into large sulfate salt and small sulfur compounds. The seasonal flux of $SO^{2-}_{4\ small}$ during the 1970s (10.8 ± 2.32 mg m^{-2} $season^{-1}$) is about three times that during the 2010s (3.30 ± 2.02 mg m^{-2} $season^{-1}$). On the other hand, the seasonal flux of $SO^{2-}_{4\ large}$ during the 1970s (1.62 ± 0.54 mg m^{-2} $season^{-1}$) is slightly lower than that during the 2010s (2.49 ± 2.00 mg m^{-2} $season^{-1}$). This small aerosol also provided the largest sulfur flux to the ice core, suggesting that the anthropogenic sulfur particles remained small during their transport (below 0.4 μm diameter) and if they were CCN, then their combination of being relatively small and numerous would imply that they had a relatively large radiative forcing. Hence, understanding the small sulfate particles is important for precise reconstruction of past aerosol radiative forcings and how the sulfate particles can cool the Arctic region.

After dividing the $SO^{2-}_{4\ large}$ seasonal fluxes into Na_2SO_4, $CaSO_4$, and $(NH_4)_2SO_4$ fluxes, we found the dominant component for $SO^{2-}_{4\ large}$ to be the $(NH_4)_2SO_4$ flux in both periods. In the 1970s, it is 1.03 ± 0.44 mg m^{-2} $season^{-1}$, and in the 2010s it is 1.48 ± 1.40 mg m^{-2} $season^{-1}$. On the other hand, the $SO^{2-}_{4\ large}$ flux increased by 154% from the 1970s (1.62 mg m^{-2} $season^{-1}$) to the 2010s (2.49 mg m^{-2} $season^{-1}$), driven mainly by an increase in Na_2SO_4 flux. Thus, the 2010s had more sulfatization of sea salt. A possible reason is that the Na_2SO_4 and $(NH_4)_2SO_4$ are independent, with different sources and transport pathways. As sulfate during the 1970s arrived from a different pathway than that of sea salt, sea-salt modification to sodium sulfate was less likely to occur.

We also ran the MRI-ESM2.0 model to simulate the contributions, both anthropogenic and natural, to the deposited sulfate flux from 1950 to 2014 in the SE-Dome region. The simulated sulfate flux of anthropogenic origin during 1973–1975 (42.6 ± 25.4 mg m^{-2} yr^{-1}) was found to be four times higher than that during 2010–2012 (10.7 ± 2.74 mg m^{-2} yr^{-1}), agreeing closely to the flux change of $SO^{2-}_{4\ small}$ from 43.36 ± 9.30 to 13.20 ± 8.06 mg m^{-2} yr^{-1} found here for these periods. Thus, the simulations support our argument that the anthropogenic SO_2

from these regions is likely to form small SO_4^{2-} liquid droplets and small sulfate salt particles due to condensation of H_2SO_4 on small particles and aqueous-phase reactions by SO_2 on aerosol-originated cloud droplets.

Data Availability Statement

Raw data from the ice core and the MRI ESM2.0 used in this study are available in the Hokkaido University Collection of Scholarly and Academic papers (Iizuka et al., 2022).

Acknowledgments
We are grateful to the drilling and initial analysis teams of SE-Dome ice core project. We also thank Chihiro Fukunaga and Yuiko Tahara (Hokkaido University) for assistance with particle measurement by SED/EDS. This research was supported by grants from JSPS KAKENHI (Numbers JP18H05292 [Y.I.], JP26257201 [Y.I.], JP17H04709 [H.M.], JP18H03363 [N.O.], JP20H04305 [S.H.], and JP16H05884 [S.H.]), and Joint Research Program and the Readership program of the Institute of Low Temperature Science, Hokkaido University. This study was a part of Arctic Challenge for Sustainability II (ArCS II, Program Grant No. JPMXD1420318865), the Environment Research and Technology Development Fund (JPMEERF20202003 and JPMEERF20205001) of the Environmental Restoration and Conservation Agency of Japan, and a grant for the Global Environmental Research Coordination System from the Ministry of the Environment, Japan (MLIT1753).

References

Aizawa, T., Oshima, N., & Yukimoto, S. (2022). Contributions of anthropogenic aerosol forcing and multidecadal internal variability to mid-20th century Arctic cooling—CMIP6/DAMIP multimodel analysis. *Geophysical Research Letters*, *49*(4), e2021GL097093. https://doi.org/10.1029/2021GL097093

Amino, T., Iizuka, Y., Matoba, S., Shimada, R., Oshima, N., Suzuki, T., et al. (2020). Annual and seasonal dust fluxes during 1960-2014 from a southeastern dome in Greenland. *Polar Science*, *27*, 100599. https://doi.org/10.1016/j.polar.2020.100599

Bauer, S. E., Tsigaridis, K., Faluvegi, G., Kelley, M., Lo, K. K., Miller, R. L., et al. (2020). Historical (1850–2014) aerosol evolution and role on climate forcing using the GISS ModelE2.1 contribution to CMIP6. *Journal of Advances in Modeling Earth Systems*, *12*(8), e2019MS001978. https://doi.org/10.1029/2019MS001978

Bory, A. J. M., Abouchami, W., Galer, S. J. G., Svensson, A., Christensen, J. N., & Biscaye, P. E. A. (2014). Chinese imprint in insoluble pollutants recently deposited in central Greenland as indicated by lead isotopes. *Environmental Science and Technology*, *48*(3), 1451–1457. https://doi.org/10.1021/es4035655

Bory, A. J. M., Biscaye, P. E., Svensson, A., & Grousset, F. E. (2002). Seasonal variability in the origin of recent atmospheric mineral dust at NorthGRIP, Greenland. *Earth and Planetary Science Letters*, *196*(3–4), 123–134. https://doi.org/10.1016/S0012-821X(01)00609-4

Boucher, O., & Anderson, T. L. (1995). GCM assessment of the sensitivity of direct climate forcing by anthropogenic sulphate aerosols to aerosol size and chemistry. *Journal of Geophysical Research*, *100*(D12), 26117–26134. https://doi.org/10.1029/95jd02531

Boyce, D. G., Lewis, M. R., & Worm, B. (2010). Global phytoplankton decline over the past century. *Nature*, *466*(7306), 591–596. https://doi.org/10.1038/nature09268

Breider, T. J., Mickley, L. J., Jacob, D. J., Wang, Q., Fisher, J. A., Chang, R. Y.-W., & Alexander, B. (2014). Annual distributions and sources of Arctic aerosol components, aerosol optical depth, and aerosol absorption. *Journal of Geophysical Research: Atmospheres*, *119*(7), 4107–4124. https://doi.org/10.1002/2013JD020996

Brock, C. A., Radke, L. F., & Hobbs, P. V. (1990). Sulphur in particles in Arctic hazes derived from airborne in situ and lidar measurements. *Journal of Geophysical Research*, *95*(D13), 22369–22387. https://doi.org/10.1029/JD095iD13p22369

Chi, J. W., Li, W. J., Zhang, D. Z., Zhang, J. C., Lin, Y. T., Shen, X. J., et al. (2015). Sea salt aerosols as a reactive surface for inorganic and organic acidic gases in the Arctic troposphere. *Atmospheric Chemistry and Physics*, *15*(19), 11341–11353. https://doi.org/10.5194/acp-15-11341-2015

Chylek, P., Vogelsang, T. J., Klett, J. D., Hengartner, N., Higdon, D., Lesins, G., & Dubey, M. K. (2016). Indirect Aerosol effect increases CMIP5 models' projected Arctic warming. *Journal of Climate*, *29*(4), 1417–1428. https://doi.org/10.1175/JCLI-D-15-0362.1

Crippa, M., Janssens-Maenhout, G., Dentener, F., Guizzardi, D., Sindelarova, K., Muntean, M., et al. (2016). Forty years of improvements in European air quality: Regional policy-industry interactions with global impacts. *Atmospheric Chemistry and Physics*, *16*(6), 3825–3841. https://doi.org/10.5194/acp-16-3825-2016

Eyring, V., Bony, S., Meehl, G. A., Senior, C. A., Stevens, B., Stouffer, R. J., & Taylor, K. E. (2016). Overview of the Coupled Model Intercomparison Project Phase 6 (CMIP6) experimental design and organization. *Geoscientific Model Development*, *9*(5), 1937–1958. https://doi.org/10.5194/gmd-9-1937-2016

Fischer, H., Siggaard-Andersen, M. L., Ruth, U., Röthlisberger, R., & Wolff, E. W. (2007). Glacial/interglacial changes in mineral dust and sea-salt records in polar ice cores: Sources, transport and deposition. *Reviews of Geophysics*, *45*(1), RG1002. https://doi.org/10.1029/2005RG000192

Fischer, H., Wagenbach, D., & Kipfstuhl, J. (1998). Sulfate and nitrate firn concentrations on the Greenland ice sheet: 2. Temporal anthropogenic deposition changes. *Journal of Geophysical Research*, *103*(D17), 21935–21942. https://doi.org/10.1029/98JD01886

Fisher, J. A., Jacob, D. J., Wang, Q., Bahreini, R., Carouge, C. C., Cubison, M. J., et al. (2011). Sources, distribution, and acidity of sulphate–ammonium aerosol in the Arctic in winter–spring. *Atmospheric Environment*, *45*(39), 7301–7318. https://doi.org/10.1016/j.atmosenv.2011.08.030

Furukawa, R., Uemura, R., Fujita, K., Sjolte, J., Yoshimura, K., Matoba, S., & Iizuka, Y. (2017). Seasonal scale dating of shallow ice core from Greenland using oxygen isotope matching between data and simulation. *Journal of Geophysical Research: Atmospheres*, *122*(20), 10873–10887. https://doi.org/10.1002/2017JD026716

Gidden, M., Riahi, K., Smith, S., Fujimori, S., Luderer, G., Kriegler, E., et al. (2019). Global emissions pathways under different socioeconomic scenarios for use in CMIP6: A dataset of harmonized emissions trajectories through the end of the century. *Geoscientific Model Development*, *12*(4), 1443–1475. https://doi.org/10.5194/gmd-12-1443-2019

Gillett, N. P., Kirchmeier-Young, M., Ribes, A., Shiogama, H., Hegerl, G., Knutti, R., et al. (2021). Constraining human contributions to observed warming since the pre-industrial period. *Nature Climate Change*, *11*(3), 207–212. https://doi.org/10.1038/s41558-020-00965-9

Gillett, N. P., Shiogama, H., Funke, B., Hegerl, G., Knutti, R., Matthes, K., et al. (2016). The Detection and Attribution Model Intercomparison Project (DAMIP v1. 0) contribution to CMIP6. *Geoscientific Model Development*, *9*(10), 3685–3697. https://doi.org/10.5194/gmd-9-3685-2016

Hara, K., Nakazawa, F., Fujita, S., Fukui, K., Enomoto, H., & Sugiyama, S. (2014). Horizontal distributions of aerosol constituents and their mixing states in Antarctica during the JASE traverse. *Atmospheric Chemistry and Physics*, *14*(18), 10211–10230. https://doi.org/10.5194/acp-14-10211-2014

Hattori, S., Iizuka, Y., Alexander, B., Ishino, S., Fujita, K., Zhai, S., et al. (2021). Isotopic evidence for acidity-driven enhancement of sulfate formation after SO_2 emission control. *Science Advances*, *7*(19), eabd4610. https://doi.org/10.1126/sciadv.abd4610

Hoesly, R. M., Smith, S. J., Feng, L., Klimont, Z., Janssens-Maenhout, G., Pitkanen, T., et al. (2018). Historical (1750–2014) anthropogenic emissions of reactive gases and aerosols from the Community Emissions Data System (CEDS). *Geoscientific Model Development*, *11*(1), 369–408. https://doi.org/10.5194/gmd-11-369-2018

Iizuka, Y., Matoba, S., Yamasaki, T., Oyabu, I., Kadota, M., & Aoki, T. (2016). Glaciological and meteorological observations at the SE-Dome site, southeastern Greenland Ice Sheet. *Bulletin of Glaciological Research*, *34*, 1–10. https://doi.org/10.5331/bgr.15R03

Iizuka, Y., Miyake, T., Hirabayashi, M., Suzuki, T., Matoba, S., Motoyama, H., et al. (2009). Constituent elements of insoluble and nonvolatile particles during the Last Glacial Maximum of the Dome Fuji ice core. *Journal of Glaciology*, *55*(191), 552–562. https://doi.org/10.3189/002214309788816696

Iizuka, Y., Miyamoto, A., Hori, A., Matoba, S., Furukawa, R., Saito, T., et al. (2017). A firn densification process in the high accumulation dome of southeastern Greenland. *Arctic Antarctic and Alpine Research*, *49*(1), 13–27. https://doi.org/10.1657/aaar0016-034

Iizuka, Y., Ohno, H., Uemura, R., Suzuki, T., Oyabu, I., Hoshina, Y., et al. (2016). Spatial distributions of soluble salts in surface snow of East Antarctica. *Tellus B: Chemical and Physical Meteorology*, *68*(1), 29285. https://doi.org/10.3402/tellusb.v68.29285

Iizuka, Y., Tsuchimoto, A., Hoshina, Y., Sakurai, T., Hansson, M., Karlin, T., et al. (2012). The rates of sea salt sulfatization in the atmosphere and surface snow of inland Antarctica. *Journal of Geophysical Research*, *117*(D4), D04308. https://doi.org/10.1029/2011JD01637

Iizuka, Y., Uemura, R., Fujita, K., Hattori, S., Seki, O., Miyamoto, C., et al. (2018). A 60 year record of atmospheric aerosol depositions preserved in a high accumulation dome ice core, Southeast Greenland. *Journal of Geophysical Research: Atmospheres*, *123*(1), 574–589. https://doi.org/10.1002/2017JD026733

Iizuka, Y., Uemura, R., Matsui, H., Oshima, N., Kawakami, K., Hattori, S., et al. (2022). Raw data for figures and table of this paper [Dataset]. Hokkaido University Collection of Scholarly and Academic Papers (HUSCAP). Retrieved from http://hdl.handle.net/2115/86374

Iizuka, Y., Uemura, R., Motoyama, H., Suzuki, T., Miyake, T., Hirabayashi, M., & Hondoh, T. (2012). Sulphate-climate coupling over the past 300,000 years in inland Antarctica. *Nature*, *490*(7418), 81–84. https://doi.org/10.1038/nature11359

Kerminen, V. M., Chen, X., Vakkari, V., Petäjä, T., Kulmala, M., & Bianchi, F. (2018). Atmospheric new particle formation and growth: Review of field observations. *Environmental Research Letters*, *13*(10), 103003. https://doi.org/10.1088/1748-9326/aadf1083c

Li, L., Chen, Z. M., Zhang, Y. H., Zhu, T., Li, J. L., & Ding, J. (2006). Kinetics and mechanism of heterogeneous oxidation of sulfur dioxide by ozone on surface of calcium carbonate. *Atmospheric Chemistry and Physics*, *6*(9), 2453–2464. https://doi.org/10.5194/acp-6-2453-2006

Mahmood, R., von Salzen, K., Norman, A.-L., Galí, M., & Levasseur, M. (2019). Sensitivity of Arctic sulfate aerosol and clouds to changes in future surface seawater dimethylsulfide concentrations. *Atmospheric Chemistry and Physics*, *19*(9), 6419–6435. https://doi.org/10.5194/acp-19-6419-2019

Mann, G. W., Carslaw, K. S., Reddington, C. L., Pringle, K. J., Schulz, M., Asmi, A., et al. (2014). Intercomparison and evaluation of global aerosol microphysical properties among AeroCom models of a range of complexity. *Atmospheric Chemistry and Physics*, *14*(9), 4679–4713. https://doi.org/10.5194/acp-14-4679-2014

Matsui, H., Hamilton, D. S., & Mahowald, N. M. (2018). Black carbon radiative effects highly sensitive to emitted particle size when resolving mixing-state diversity. *Nature Communications*, *9*, 1. https://doi.org/10.1038/s41467-018-05635-1

Meinshausen, M., Vogel, E., Nauels, A., Lorbacher, K., Meinshausen, N., Etheridge, D. M., et al. (2017). Historical greenhouse gas concentrations for climate modelling (CMIP6). *Geoscientific Model Development*, *10*(5), 2057–2116. https://doi.org/10.5194/gmd-10-2057-2017

Miyamoto, C., Iizuka, Y., Matoba, S., Hattori, S., & Takahashi, Y. (2022). Gypsum formation from calcite in the atmosphere recorded in aerosol particles transported and trapped in Greenland ice core sample is a signature of secular change of SO_2 emission in East Asia. *Atmospheric Environment*, *278*, 119061. https://doi.org/10.1016/j.atmosenv.2022.119061

Moore, R. H., Bahreini, R., Brock, C. A., Froyd, K. D., Cozic, J., Holloway, J. S., et al. (2011). Hygroscopicity and composition of Alaskan Arctic CCN during April 2008. *Atmospheric Chemistry and Physics*, *11*(22), 11807–11825. https://doi.org/10.5194/acp-11-11807-2011

Mulvaney, R., Wolff, E. W., & Oates, K. (1988). Sulphuric acid at grain boundaries in Antarctic ice. *Nature*, *331*(6153), 247–249. https://doi.org/10.1038/331247a0

Ohno, H., Igarashi, M., & Hondoh, T. (2005). Salt inclusions in polar ice core: Location and chemical form of water-soluble impurities. *Earth and Planetary Science Letters*, *232*(1–2), 171–178. https://doi.org/10.1016/j.epsl.2005.01.001

Oshima, N., Yukimoto, S., Deushi, M., Koshiro, T., Kawai, H., Tanaka, T. Y., & Yoshida, K. (2020). Global and Arctic effective radiative forcing of anthropogenic gases and aerosols in MRI-ESM2.0. *Progress in Earth and Planetary Science*, *7*(1), 38. https://doi.org/10.1186/s40645-020-00348-w

Osman, M. B., Das, S. B., Trusel, L. D., Evans, M. J., Fischer, H., Grieman, M. M., et al. (2019). Industrial-era decline in subarctic Atlantic productivity. *Nature*, *569*(7757), 551–555. https://doi.org/10.1038/s41586-019-1181-8

Park, R. J., Jacob, D. J., Field, B. D., Yantosca, R. M., & Chin, M. (2004). Natural and transboundary pollution influences on sulphate-nitrate-ammonium aerosols in the United States: Implications for policy. *Journal of Geophysical Research*, *109*(D15), D15204. https://doi.org/10.1029/2003jd004473

Polyakov, I. V., Alekseev, G. V., Bekryaev, R. V., Bhatt, U., Colony, R. L., Johnson, M. A., et al. (2002). Observationally based assessment of polar amplification of global warming. *Geophysical Research Letters*, *29*(18), 1878–25-4. https://doi.org/10.1029/2001GL011111

Reddington, C. L., Carslaw, K. S., Spracklen, D. V., Frontoso, M. G., Collins, L., Merikanto, J., et al. (2011). Primary versus secondary contributions to particle number concentrations in the European boundary layer. *Atmospheric Chemistry and Physics*, *11*(23), 12007–12036. https://doi.org/10.5194/acp-11-12007-2011

Roelofs, G. J., Stier, P., Feichter, J., Vignati, E., & Wilson, J. (2006). Aerosol activation and cloud processing in the global aerosol-climate model ECHAM5-HAM. *Atmospheric Chemistry and Physics*, *6*(9), 2389–2399. https://doi.org/10.5194/acp-6-2389-2006

Schulz, M., Chin, M., & Kinne, S. (2009). *The aerosol model comparison Project, AeroCom, phase II: Clearing up diversity* (Vol. 41). IGAC Newsletter.

Schulz, M., Textor, C., Kinne, S., Balkanski, Y., Bauer, S., Berntsen, T., et al. (2006). Radiative forcing by aerosols as derived from the AeroCom present-day and pre-industrial simulations. *Atmospheric Chemistry and Physics*, *6*(12), 5225–5246. https://doi.org/10.5194/acp-6-5225-2006

Seguin, A. M., Norman, A. L., & Barrie, L. (2014). Evidence of sea ice source in aerosol sulphate loading and size distribution in the Canadian high Arctic from isotopic analysis. *Journal of Geophysical Research: Atmospheres*, *119*(2), 1087–1096. https://doi.org/10.1002/2013JD020461

Seguin, A. M., Norman, A.-L., Eaton, S., & Wadleigh, M. (2011). Seasonality in size segregated biogenic, anthropogenic and sea salt sulphate aerosols over the North Atlantic. *Atmospheric Environment*, *45*(38), 6947–6954. https://doi.org/10.1016/j.atmosenv.2011.09.033

Shindell, D., & Faluvegi, G. (2009). Climate response to regional radiative forcing during the twentieth century. *Nature Geoscience*, *2*(4), 473–300. https://doi.org/10.1038/ngeo473

Sirois, A., & Barrie, L. A. (1999). Arctic lower tropospheric aerosol trends and composition at Alert, Canada: 1980-1995. *Journal of Geophysical Research*, *104*(D9), 11619–11631. https://doi.org/10.1029/1999jd900077

Smith, C. J., Kramer, R. J., Myhre, G., Alterskjær, K., Collins, W., Sima, A., et al. (2020). Effective radiative forcing and adjustments in CMIP6 models. *Atmospheric Chemistry and Physics*, *20*(16), 9591–9618. https://doi.org/10.5194/acp-20-9591-2020

Szopa, S., Naik, V., Adhikary, B., Artaxo, P., Berntsen, T., Collins, W. D., et al. (2021). Short-lived climate forcers. In V. P. Zhai, A. Pirani, S. L. Connors, C. Péan, S. Berger, et al. (Eds.), *Climate change 2021: The physical science basis. Contribution of working group I to the sixth*

assessment report of the intergovernmental panel on climate change [Masson-Delmotte] (pp. 817–922). Cambridge University Press. https://doi.org/10.1017/9781009157896.008

Takahashi, Y., Miyoshi, T., Higashi, M., Kamioka, H., & Kanai, Y. (2009). Neutralization of calcite in mineral aerosols by acidic sulphur species collected in China and Japan studied by Ca K-edge X-ray absorption near-edge structure. *Environmental Science & Technology*, *43*(17), 6535–6540. https://doi.org/10.1021/es9010256

Takemura, T. (2020). Return to different climate states by reducing sulfate aerosols under future CO_2 concentrations. *Scientific Reports*, *10*(1), 21748. https://doi.org/10.1038/s41598-020-78805-1

Thomason, L. W., Ernest, N., Millán, L., Rieger, L., Bourassa, A., Vernier, J. P., et al. (2018). A global space-based stratospheric aerosol climatology: 1979 – 2016. *Earth System Science Data*, *10*(1), 469–492. https://doi.org/10.5194/essd-10-469-2018

Udisti, R., Bazzano, A., Becagli, S., Bolzacchini, E., Caiazzo, L., Cappelletti, D., et al. (2016). Sulphate source apportionment in the Ny-Ålesund (Svalbard Islands) Arctic aerosol. *Rendiconti Lincei*, *27*(1), 85–94. https://doi.org/10.1007/s12210-016-0517-7

van Marle, M. J. E., Kloster, S., Magi, B. I., Marlon, J. R., Daniau, A. L., Field, R. D., et al. (2017). Historic global biomass burning emissions for CMIP6 (BB4CMIP) based on merging satellite observations with proxies and fire models (1750–2015). *Geoscientific Model Development*, *10*(9), 3329–3357. https://doi.org/10.5194/gmd-10-3329-2017

von Schuckmann, K., Traon, P. Y. L., Smith, N., Pascual, A., Brasseur, P., Fennel, K., et al. (2018). Copernicus marine Service ocean state report. *Journal of Operational Oceanography*, *11*(sup1), 2018. https://doi.org/10.1080/1755876x.2018.1489208

Wolff, E. W., Fischer, H., Fundel, F., Ruth, U., Twarloh, B., Littot, G. C., et al. (2006). Southern Ocean sea-ice extent, productivity and iron flux over the past eight glacial cycles. *Nature*, *440*(7083), 491–496. https://doi.org/10.1038/nature04614

Yukimoto, S., Kawai, H., Koshiro, T., Oshima, N., Yoshida, K., Urakawa, S., et al. (2019). The meteorological research Institute Earth system model version 2.0, MRI-ESM2.0: Description and basic evaluation of the physical component. *Journal of the Meteorological Society of Japan*, *97*(5), 931–965. https://doi.org/10.2151/jmsj.2019-051